Wet Granular Flows in a Bladed Mixer: Experiments and Simulations of Monodisperse Spheres

Brenda Remy
Late Phase Chemical Development, Bristol-Myers Squibb Co., New Brunswick, NJ 08903

Dept. of Chemical and Biochemical Engineering, Rutgers University, Piscataway, NJ 08854

Johannes G. Khinast
Institute for Process Engineering, Graz University of Technology, Graz A-8010, Austria

Benjamin J. Glasser
Dept. of Chemical and Biochemical Engineering, Rutgers University, Piscataway, NJ 08854

DOI 10.1002/aic.13743
Published online April 9, 2012 in Wiley Online Library (wileyonlinelibrary.com).

The flow and agglomeration of wet particles in a bladed mixer was studied experimentally using particle image velocimetry and computationally using the discrete element method. The experimental and computational work showed that particle beds at low moisture contents are characterized by enhanced convective and diffusive particle motion as well as enhanced mixing kinetics when compared to dry particle beds. This behavior is attributed to the development of small particle agglomerates which behave like rough, nonspherical particles and enable the transfer of energy from the blades to the particle bed. At higher moisture contents, a different behavior was observed. Particle convective and diffusive motion was hindered by the presence of moisture at higher levels leading to a decrease in mixing performance. This occurs as large agglomerates are formed and are not broken apart by shear leading to poor mixing. Pressure and shear stress profiles were shown to be affected by the amount of moisture in the system. The extent of agglomeration at different moisture contents was quantified via the discrete element simulations. Agglomerate size distributions and morphology were shown to be strong functions of moisture content. © 2012 American Institute of Chemical Engineers *AIChE J,* 58: 3354–3369, 2012
Keywords: bladed mixer, agitated drying, wet granular flow and particle agglomeration

Introduction

The presence of interparticle cohesive forces is often encountered in many practical granular systems. These forces give rise to different phenomenological behaviors in cohesive granular materials from what is observed in noncohesive systems. For example, the tensile strength of static piles increases in the presence of cohesion.[1] This characteristic enables the creation of sand castles from wet sand since a stable shape cannot be created with dry sand.[2] The angle of repose of a granular pile is usually increased by cohesion.[3] Cohesive forces can increase dilation of granular materials during flow and can induce hysteresis.[4,5] The apparent friction between particles increases even with a small amount of cohesion in the system.[6] This complex behavior makes the prediction and control of cohesive granular flows difficult. The presence of cohesion in industrial scenarios leads to operational problems which are not easily solved or prevented. Cohesion can often lead to problems such as bridging, channeling, discontinuous mass flows, material accumulation on equipment walls and broadening of particle-size distributions[7,8] due to the formation of particle agglomerates. The majority of research in granular flows has focused on noncohesive systems. Studies involving the flow of cohesive granular materials are not as commonly encountered in the literature. The need for fundamental studies dealing with the transport and storage of cohesive granular materials is therefore substantial.

The presence of moisture in a granular system gives rise to cohesion due to capillary forces. When particles are in contact in wet systems, a meniscus is formed between the contacting surfaces as capillary action attracts the liquid on the nearby surfaces.[9] This leads to the formation of a liquid bridge which creates an attractive force due to surface tension and the hydrostatic pressure inside the bridge.[10] Capillary forces can have a significant effect on the behavior of granular materials. For example, the magnitude of capillary forces can be double that of gravity for particles with a diameter above 100 μm.[3] Particles in a wet system can exist in a number of different states depending on the moisture content of the system. These states are the pendular state (low moisture content), the funicular state (intermediate moisture content), and the capillary state (high moisture contents).[11] The resulting behavior in wet systems is dictated by the amount of liquid present in the system and the distribution of the liquid via capillary bridge networks.[3] The

Correspondence concerning this article should be addressed to B. Remy at bglasser@rutgers.edu.

presence of moisture also leads to the development of viscous forces as particles move past one another. However, at low moisture contents, the effect of these forces is secondary to the effect of capillary forces.[12]

Bladed mixers are commonly used in a variety of industrial processes as these units are capable of handling materials ranging from free flowing beds to cohesive systems.[13] These mixers are frequently encountered in the food, bulk chemical and pharmaceutical industries. Some industrial applications of bladed mixers include wet granulation,[14–16] agitated drying,[17–19] and mixing and blending.[20] For bladed mixers, the majority of past studies have focused on dry granular flows.[21–24] These studies have provided insight on the flow patterns and velocity profiles that develop inside bladed mixer for a wide range of particle properties and operating conditions. However, the case of granular flow in bladed mixers in the presence of cohesion has received less attention despite the fact that cohesion is present in many industrial scenarios where bladed mixers are used (i.e., wet granulation, agitated drying). Most of the research on wet granular flows has been performed for prototypical geometries such as simple shear flows,[25,26] discharging hoppers,[27] or rotating drums.[28,29] It remains unclear whether the results obtained in these simple geometries could be extended to more complex systems such as bladed mixers.

Several researches have studied wet bladed mixer flows in the area of wet granulation.[30–32] These studies, however, focused mostly on the effect of liquid distribution and operating parameters on resulting granule properties. Few fundamental studies are found in the literature which investigate the flow and mixing of wet particle beds in bladed mixers. Lekhal et al.[33] experimentally examined the effect of moisture on granular flows in a bladed mixer. Two flow regimes were identified at different levels of bed moisture. At low moisture contents, granular flow was dominated by the motion of individual grains, while at high moisture contents the flow is controlled by the motion of small agglomerates that formed due to cohesive forces. More recently Radl et al.[34] used the discrete element method (DEM) to study bladed flows of spherical particles in the millimeter size range at low moisture contents (<1 v/v %). The authors found that the presence of moisture led to increased dilation of the particle bed as the blades were rotated. Additionally, the authors observed increased particle velocities and granular temperatures for the wet particle beds which led to enhanced localized mixing rates when compared to dry particle beds. These studies have provided an initial understanding on how wet flows develop inside bladed mixers but have not clearly correlated the effect of moisture content and particle properties on macroscopic properties like void fraction, pressure, stress and degree of mixing. Additionally, little is currently known about the effect of moisture content on the formation of particle agglomerates. While wet granulation processes are designed to achieve particle size enlargement via agglomeration, agitated drying processes are generally designed to minimize the extent of agglomerate formation. Uncontrolled agglomeration of the particle bed could lead to broader particle-size distributions and could ultimately lead to the production of out-of-specification batches.

This study focuses on the experimental and computational examination of wet particle flows at different moisture contents in a bladed mixer. Moisture contents ranging from 1.0 to 4.5 v/v % were examined experimentally and computationally. This range was chosen to ensure that the liquid bridges exist in the pendular regime.[35,36] Experimental flows were characterized with the use of the Particle Image Velocimetry (PIV) technique. DEM simulations were carried out which included the effect of cohesion due to capillary liquid bridges. Our bladed mixer consists of a vertical cylinder mechanically agitated by four blades pitched at a 45° angle. This geometry is representative of several industrial bladed mixer units, including agitated dryers and wet granulators. We include a detailed comparison between experimental results and the computational results. The effect of moisture content on macroscopic quantities like flow patterns, mixing kinetics, bulk density, stress and particle diffusivities is discussed. The effect of moisture content on particle agglomeration is then discussed. The findings presented are relevant to the operation and optimization of industrial processes as they provide insight on parameters that affect particle velocities, mixing and particle agglomeration in an industrially relevant geometry.

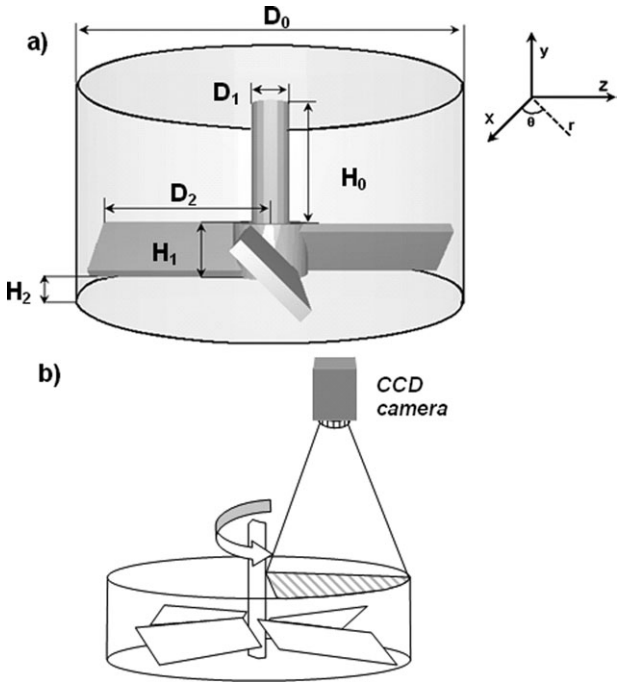

Figure 1. Bladed mixer geometry.

(a) mixer schematic and (b) laboratory PIV set-up.

Experimental Method

Experimental set-up

The geometry of the bladed mixer used in this work is shown in Figure 1. The dimensions for the mixer are shown in Table 1. The laboratory unit consisted of a glass cylindrical vessel agitated by an impeller with a glass shaft and 4 Teflon® blades pitched at a 45° angle. The blades were rotated in the counterclockwise direction leading to an obtuse configuration. The granular material used in this work was Dragonite® glass beads (Jaygo, Union, NJ) with diameters of 2 mm (±0.3 mm). For all experiments, the granular material was loaded into the laboratory mixer to an initial bed height of ~30 mm. This bed height was sufficient to cover the top tip of the blades.

The PIV technique was used to measure surface particle velocities in the laboratory unit. This technique allows for the tracking of particles in a granular bed from high-speed CCD images. A high-speed camera is placed directly above

Table 1. Mixer Dimensions Used for the PIV Experiments and the DEM Simulations

Dimension	Value (mm)
D_0	315
D_1	32.5
D_2	152.5
H_0	55
H_1	45
H_2	0

one quadrant of the flow in the bladed mixer and is used to record images of the free-surface at 250 frames per second. PIV yields both instantaneous and mean velocity vector fields for 2-D flow structures at the bed top free surface. The top surface image spans the entire radius of the container. Analysis of the PIV data was performed following the procedure outlined by Remy et al.[20] Experimental velocities were measured only near the top free surface as shown in Figure 1b. We were not able to obtain side view velocity measurements due to particles sticking to the cylinder wall in the presence of moisture.

For the wet particle experiments, the particles were first loaded into the mixer. The blades were then set to rotate counterclockwise and water was added from the top at different locations with the use of a small spraying device. The impeller was driven by a motor with a speed controller with an accuracy of ± 0.1 rpm under load. The wet particle bed was allowed to mix for 5 minutes before taking the PIV measurements. This water addition procedure was found to yield reproducible results in the laboratory and is consistent with the procedure used by Lekhal et al.[33] Experiments were performed using a blade speed of 25 rpm.

Discrete Element Method

Contact force model

PIV experimental measurements are limited to two-dimensional flow fields near free surfaces. However, a complete three-dimensional (3-D) picture can be obtained with the use of DEM simulations. This technique can reveal a greater level of detail of how granular flows develop in complex equipment configurations since it allows for the study of parameters that are difficult to measure or vary experimentally. Information on localized flow, contact network structures and stress profiles can be easily obtained via DEM simulations. These parameters, however, are difficult if not impossible to obtain experimentally.

In DEM simulations, the behavior of a particle bed is determined by resolving the contact forces that develop between neighboring particles. From the interparticle contact forces, the trajectory of each particle can be obtained by integrating Newton's equations of motion starting from an initial system configuration. For a wet granular system in the pendular state, the motion of each particle is described by

$$m_i \frac{dv_i}{dt} = \sum_j (F_{ij}^N + F_{ij}^T) + F_{ij}^c + m_i g \tag{1}$$

$$I_i \frac{d\omega_i}{dt} = \sum_j (R_i \times F_{ij}^T) + \tau_{rij} \tag{2}$$

where m_i, R_i, I_i, v_i, and ω_i are the mass, radius, moment of inertia, linear velocity and angular velocity of particle i, and g is the acceleration due to gravity. F_{ij}^N and F_{ij}^T are the normal and tangential forces, respectively, resulting from the contact of particle i with particle j. F_{ij}^C is the cohesive force experienced by particle i due to the formation of a liquid bridge between it and particle j.

The contact forces are determined from the model proposed by Tsuji et al.[37] Our previous bladed mixer work has demonstrated ability of this model to produce DEM results in good agreement with experimental data for dry, monodisperse flows.[20] The EDEM software (version 2.1) from DEM Solutions was used to perform the simulations. A detailed description of the contact model used in this work can be found in Remy et al.[22]

Cohesive force model

The cohesion force model proposed by Mikami et al.[38] was used in this work. A custom code was developed to include the cohesion model calculations in the EDEM software with the used of the extended API feature of the software. This model is based on regression expressions obtained from numerical solutions of the Laplace-Young equation. From this model, the cohesion force is given by

$$\widehat{F^c} = \exp(A\widehat{h} + B) + C \tag{3}$$

$$A = -1.1\widehat{V}^{-0.53} \tag{4}$$

$$B = (-0.34 \ln \widehat{V} - 0.96)\theta^2 - 0.019 \ln \widehat{V} + 0.48 \tag{5}$$

$$C = 0.0042 \ln \widehat{V} + 0.0078 \tag{6}$$

where $\widehat{F^c}$ is the normalized capillary force ($\widehat{F^c} = F^c/2\pi R\gamma$), γ, γ is the surface tension of the liquid, $\widehat{V}$ is the dimensionless liquid bridge volume ($\widehat{V} = V/R^3$), θ is the contact angle of the liquid bridge, $\widehat{h}$ is the dimensionless separation distance between the surface of the particles ($\widehat{h} = h/R$); and A, B, and C are constants. The Mikami model has been shown to yield capillary forces in the pendular regime in good agreement with experimental data and with other numerical solutions of the Laplace-Young equation.[10,39]

When pendular bridges are stretched, the thickness of the liquid layer decreases eventually leading to the rupture of the liquid bridge. The distance at which a pendular bridge breaks is determined by using the expression proposed by Lian et al.[40]

$$\widehat{h}_c = (0.62\theta + 0.99)\widehat{V}^{0.34} \tag{7}$$

The presence of moisture also leads to the development of viscous forces between particles. The capillary number relates the magnitude of the viscous force to the capillary forces in a liquid bridge, and is calculated by

$$Ca = \eta U/\gamma \tag{8}$$

where η is the dynamic viscosity of the liquid and U is the characteristic velocity. For a water wet granular material flowing at a velocity of 0.2 m/sec (a typical velocity in a bladed mixer at the blade speed used here), the value of the capillary number is $Ca < 0.01$. This indicates that the effect of the viscous forces is negligible compared to the effect of the capillary forces. The effect of dynamic viscous forces was not be considered in this work.

Table 2. Contact Force Model Input Parameters

Variable	Symbol	Value
Rolling friction coefficient	μ_r	0.005
Sliding friction coefficient	μ_s	0.5
Particle density	ρ_p	2.2 g/ml
Young's modulus	E	2.6×10^6 Pa
Coefficient of restitution	e	0.6
Particle diameter (d)	d	2 mm
Number of particles	N	28,000
Poisson's ratio	σ	0.25
Time step		$<1 \times 10^{-5}$ sec

The following assumptions were made in the implementation of the liquid bridge model into the DEM algorithm:

(1) The total amount of liquid in the system is perfectly mixed throughout the entire particle bed such that each liquid bridge has the same volume of liquid.

(2) No condensation or evaporation of the liquid occurs.

(3) A pendular liquid bridge is formed at the point of contact when two particles come in contact. The liquid bridge continues to act between the two particles until the distances between the particles exceeds h_c.

(4) A pendular liquid bridge is formed at the point of contact when a particle comes in contact with the walls. The liquid bridge continues to act until the distance between the particle and wall exceeds h_c.

(5) Liquid bridges move tangentially slipping over the surface of the particles and the walls (i.e., the capillary force acts only in the normal direction).

In the past researchers have demonstrated that particle surface roughness could affect the magnitude of capillary forces at low liquid content.[3] In this work, however, we have not included the effect of particle surface roughness on the magnitude of the capillary forces as a first approximation. This is equivalent to assuming that the surface asperities of the particles are completely covered by the liquid layer making the particles appear smooth and completely wettable. As denoted by Herminghaus,[3] this represents an idealized system. Further work is needed to study the effect of surface roughness on the results shown here.

Mixer geometry and input parameters

DEM simulations were carried out using the dimensions listed in Table 1 together with 2 mm particles to enable a one-to-one comparison between the experimental and numerical results. The input parameters used in the calculation of the contact forces are listed in Table 2 and are, in general, those of glass beads. These input parameters were chosen since we have been shown that these values afford DEM results in good agreement with experimental results for dry flows of 2 mm glass beads in bladed mixers.[20] The value of Young's modulus was decreased from that of glass beads to reduce computational time. Parametric sensitivity studies in dry systems showed that reducing the value of Young's modulus had a negligible effect on flow patterns, velocity profiles and interparticle shear stresses. The parametric studies also showed that the value of the coefficient of restitution had a negligible effect on the results obtained in our bladed mixer. The parameters listed in Table 2 were used for the particles, the blades and cylinder walls in all the simulations. DEM simulations were performed with a blade speed of 25 rpm, similar to what was done in the experiments.

The input parameters used for the capillary liquid bridge model are listed in Table 3. The liquid properties are those of water. A contact angle of $\theta = 0^\circ$ was used as this simulates the formation of liquid bridges in hydrophylic materials.[28] It should be noted that contact angle is only dependent on material properties of the particles and the walls[9] and is not expected to change with separation distance. Further work is needed to explore the effect of contact angle on the results reported shown here. The amount of liquid in the system is characterized by the liquid volume fraction, ϕ_{liq}, which is defined as the ratio of total volume of liquid in the system to the total volume of the particles. Systems with ϕ_{liq} equal to 0, 0.01, 0.024 and 0.045 were studied. By assuming a perfect distribution of liquid within the particle bed, the value of $\widehat{V}$ can be calculated. For an average particle coordination number of 5 (typical in dry bladed mixer flows at the blade speed used here), the ϕ_{liq} values listed above are equivalent to $\widehat{V}$ values of 0, 0.018, 0.04 and 0.075 respectively. The amount of liquid in each liquid bridge is assumed to be constant in all the simulations (i.e., the $\widehat{V}$ value is the same for each particle-particle and particle-wall contact). It should be noted that the amount of liquid in each liquid bridge might not be constant in an experimental system. Scheel et al.[41] have shown that a distribution of liquid bridge volume can exist in wet systems. Here we have assumed a constant $\widehat{V}$ value as a first approximation. As such, each liquid bridge contains roughly 20% of the liquid layer of each particle. This is similar to the approach taken by Shi and McCarthy[42] and Anad et al.[36] Further work is needed to explore the effect of liquid distribution on the results reported here. Table 3 list the value of the Bond number for the simulations and for the experiments. The Bond number is the ratio of the cohesive force to the gravitational force ($Bo = 3\gamma/2R^2\rho_p g$).[43] In all the experiments and the simulations the magnitude of the cohesive force is ~5 times that of the force due to gravity.

In the coordinate system used in this work, the origin is located at the center of the cylinder's bottom plate. The amount of particles present in each simulation was enough to cover the height of the blades, similar to the experiments. In the DEM simulations, the particles were assumed to be monodisperse. Particles are created in the computational space and allowed to settle under gravity while the blades remain stationary. Blade movement is started once particle creation and deposition has been completed. Measurements are taken after the system has reached steady-state, which in our system occurs within 2 sec (~1 rotation) after commencement of blade rotation.

Results and Discussion

DEM results vs. experimental results

In this section, we compare the particle velocity profiles obtained from the DEM simulations to those obtained

Table 3. Cohesive Force Model Input Parameters

Variable	Symbol	Value
Liquid surface tension	γ	0.073 N/m
Contact angle	θ	0°
Liquid density	ρ_{liq}	1.0 g/ml
Liquid volume fraction	ϕ_{liq}	0–0.045
Dimensionless liquid bridge volume	$\widehat{V}$	0–0.075
Bond number	Bo	5

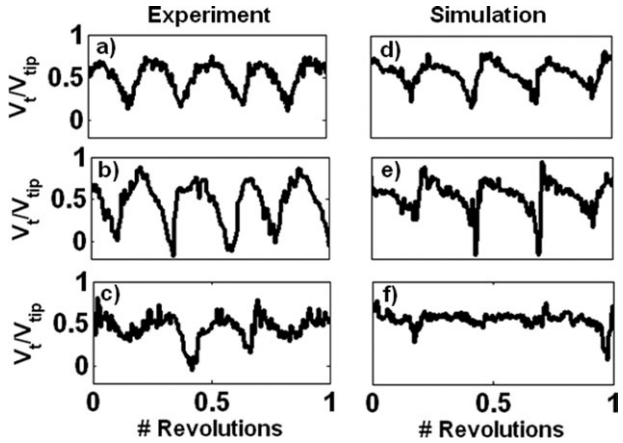

Figure 2. Tangential velocity fluctuations near top free surface at $r/R = 0.5$.

Experimental results: (a) dry, (b) $\phi_{liq} = 0.024$, and (c) $\phi_{liq} = 0.045$. Simulation results: (d) dry, (e) $\phi_{liq} = 0.024$, and (f) $\phi_{liq} = 0.045$.

experimentally. Figure 2 shows instantaneous tangential velocity profiles obtained for the PIV experiments and the DEM simulations at different liquid contents. Here, the tangential velocities have been normalized by the tip speed of the blades, V_{tip}. For both the experiments and the simulations, a 10 mm x 10 mm square control area was created at the top free surface at $r/R = 0.5$. The instantaneous velocity components were calculated by averaging over the control area at a particular time. For the DEM simulation, only the velocities of the particles located 0.75 particle diameters away from the top surface were included in the calculation. In general, good qualitative agreement is obtained between the experimental instantaneous velocities and the simulation velocities. For the dry velocity profiles (Figures 2a for the experiment and 2d and for the simulation), periodic velocity fluctuations are observed. A Fast Fourier Transform (FFT) analysis of the tangential velocity profiles revealed that the main frequency of the fluctuation is equal to the rotation frequency of the blades for both the experiment and the simulation. Normalized tangential velocity values fluctuate between 0.75 and 0.1 for both the experiment and the simulation.

Addition of water changes the tangential velocity profiles significantly. Figures 2b (experiment) and 2e (simulation) show the tangential velocities obtained for $\phi_{liq} = 0.024$. The presence of water leads to an increase in the amplitude of the velocity fluctuations. Maximum tangential velocity values are close to the tip speed of the blades for both the experiment and the simulation. Negative tangential velocities are also observed. Similar results were observed by Lekhal et al.[33] for the flow of wet art sand in a four-bladed mixer at similar moisture contents. The increase in velocity fluctuations suggest that particle movement in the tangential direction is therefore less uniform for the $\phi_{liq} = 0.024$ system compared to the dry system. In the wet systems, particle agglomeration occurs due to the presence of cohesive forces. The formation of these agglomerates leads to an increase in velocity fluctuations and a less uniform flow field.

Further addition of water leads to a different effect in the tangential velocity. Figures 2c (experiment) and 2f (simulation) show the tangential velocities obtained at $\phi_{liq} = 0.045$. At this moisture content, the periodicity displayed is less than what's observed in the dry and $\phi_{liq} = 0.024$ profiles as determined by a FFT analysis of the velocity profiles. The amplitude of the velocity fluctuation is also significantly reduced. A similar behavior was observed by Lekhal et al.[33] at high moisture contents. Inspection of the video footage obtained from the PIV experiment and the DEM simulation showed that the reduction in velocity fluctuations is due to the agglomeration of a large portion of the particle bed in front of the blades. These agglomerated particles follow the movement of the blades leading to a more uniform tangential velocity profile inside the mixer. This will be discussed further later in this article.

While the wet particle DEM simulations are able to capture the qualitative behavior observed in the experiments, some differences are observed. In particular, the amount of periodicity and the amplitude of the velocity fluctuations in the experimental results (Figures 2b, c) are higher than what is observed in the simulation results (Figures 2e, f). The differences are more pronounced for the $\phi_{liq} = 0.045$ simulation. These differences could be caused by a number of factors such as differences in particle properties, wall friction and slight polydispersity (present in the glass beads used, but not accounted for in the simulations). Additionally, in the simulations the water present in the system is assumed to uniformly coat the particles and to be perfectly mixed within the particle bed leading to a constant liquid volume in all the capillary bridges. Visual inspection of the particle bed during the experiments suggest that, while a good distribution of the water within the mixer is achieved, water is not perfectly dispersed in the mixer. In particular, water accumulates toward the bottom plate of the cylinder and this effect is more pronounced at the higher moisture contents. This is due to the effect of gravity which causes some of the water to drain out of the liquid bridges due to the low viscosity of water. Donahue et al.[44] demonstrated the reduction of volume in a liquid bridge due to gravity for two 1 inch steel spheres wetted with oil. In this work, additional experiments were conducted for particles wetted with water/glycerin mixtures at different viscosities (but equivalent liquid contents and surface tension). These experiments showed that the amount of liquid that accumulated towards the bottom was reduced as viscosity was increased. The velocity fluctuations obtained for the higher viscosity experiments resemble those obtained for the $\phi_{liq} = 0.045$ water simulation.

Figure 3 shows the experimental and simulation instantaneous radial velocity profiles obtained at different moisture

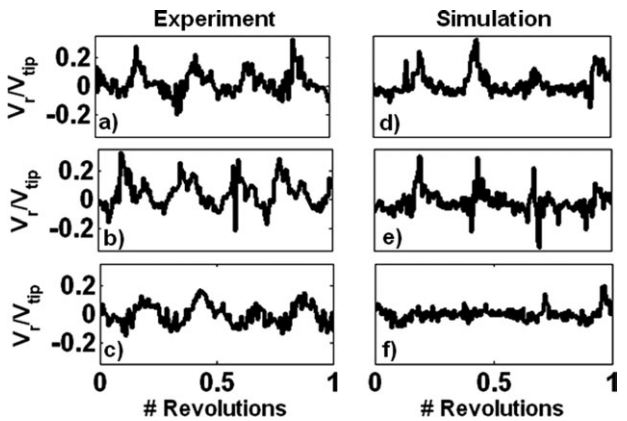

Figure 3. Radial velocity fluctuations near top free surface at $r/R = 0.5$.

Experimental results: (a) dry, (b) $\phi_{liq} = 0.024$, and (c) $\phi_{liq} = 0.045$. Simulation results: (d) dry, (e) $\phi_{liq} = 0.024$, and (f) $\phi_{liq} = 0.045$.

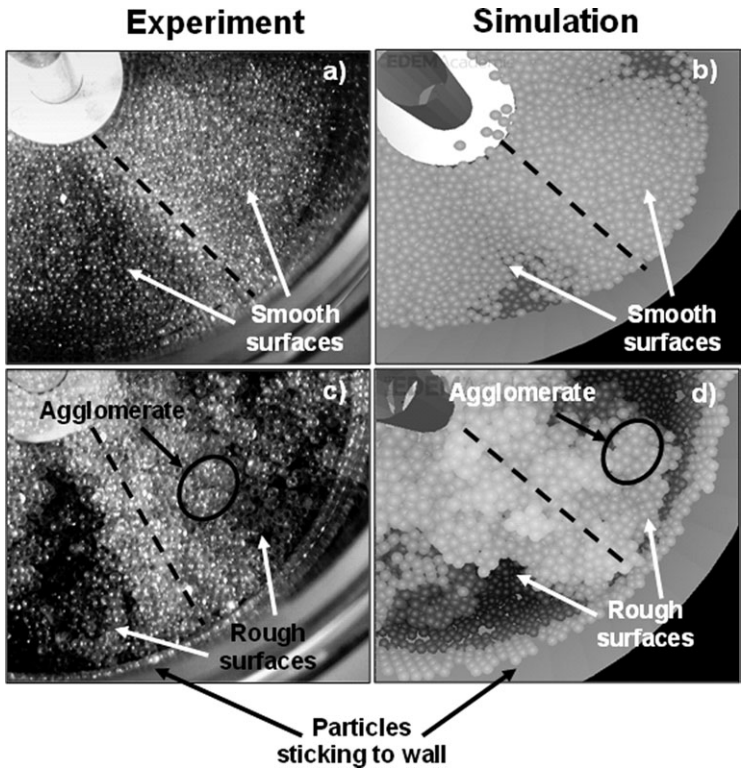

Figure 4. Deformation of particle bed near top free surface.

Dry: (a) experiment and (b) simulation. $\phi_{liq} = 0.045$: (c) experiment and (d) simulation. The dashed lines show the position of the blade. The particles in the simulation snapshots are colored according to their potential energy.

contents. The radial velocity profiles show similar trends to the tangential velocity profiles. For the dry cases (Figure 3a for the experiment and 3d for the simulation) radial velocities oscillate between positive and negative values with a frequency equal to that of the blade rotation. These fluctuations arise from the development of secondary flow structures within the mixer.[45] The amplitude of these fluctuations increases for the cases with $\phi_{liq} = 0.024$ (Figure 3b for the experiment and 3e for the simulation). A similar trend was observed by Lekhal et al.[33] at low moisture contents. These results suggest that the intensity of the secondary flow structures increases at low moisture contents. However, Figures 3c (experiment) and 3f (simulation) show that for $\phi_{liq} = 0.045$, the amplitude of the radial velocity fluctuations decreases. While addition of a small amount of water promotes the formation of stronger secondary flow patterns, too much water could hinder the formation of such flow features. The $\phi_{liq} = 0.045$ simulation over-predicts the reduction in radial velocity fluctuations when compared to the experimental results. This is most likely due to the accumulation of water towards the bottom of the cylinder during the experiments at higher moisture contents which is not accounted for in the simulations.

For dry systems with fill levels just covering the height of the blades, the granular bed deforms by forming heaps where the blades are present and valleys in between blade passes. The formation of these heaps is a key feature for dry flows in the quasi-static regime.[45] The effect of moisture on the deformation of the particle bed near the top free surface is shown in Figure 4. Experimental snapshots are displayed in Figures 4a (dry) and 4c ($\phi_{liq} = 0.045$). Simulation snapshots are presented in Figures 4b (dry) and 4d ($\phi_{liq} = 0.045$). The dashed lines show the position of the blade. The particles in the simulation snapshots are colored according to their potential energy (i.e., vertical height). It should be noted that the color differences in the gray scale observed in the experimental snapshots are due to the differences in heap height and the lighting used when these images were captured. The coloring scheme of the particles in the simulation snapshots was chosen to match this effect. For the dry cases, a smooth surface is obtained as the particles rise in front of the blade to form a heap. The free surface of the bed remains relatively flat on each side of the heap. However, at $\phi_{liq} = 0.045$, a rough surface develops due to the formation of particle agglomerates. A large portion of the particle bed forms agglomerates in front of the blades in the presence of moisture leading to the formation of larger voids on both sides of the heap. This effect is observed in both the experiment and the simulation. Additionally, the presence of moisture causes the particles closest to the side wall to stick to the cylinder walls as the blades rotate. The DEM simulation is able to capture this behavior well. Due to the high surface tension of water, the cohesive force between the particles and the wall is higher (about five times higher) than the weight of the particles causing them to stick to the walls.

Despite the discrepancies observed, the general trends obtained for both the experiments and the simulation are similar. The DEM simulations qualitatively capture the effect of moisture at different levels on the instantaneous and average particle velocities, and on the deformation of the particle bed. The remainder of this work focuses on the examination of moisture content effects via DEM simulations.

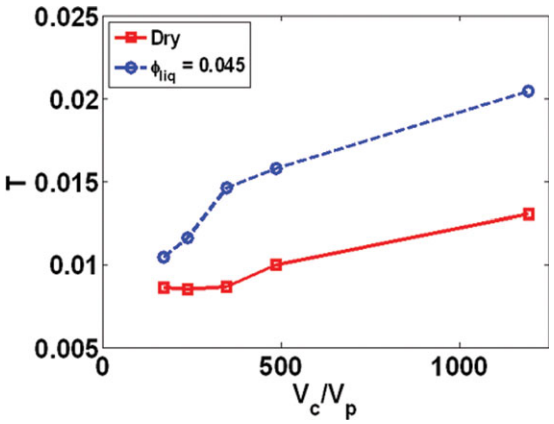

Figure 5. Effect of control volume size on time averaged granular temperature for dry and ϕ_{liq} = 0.045 cases from DEM simulations.

Granular temperature values shown here have been normalized by V_{tip}^2 and were obtained by averaging the fluctuation velocity in the tangential, radial and vertical directions for all the particles present in the computational domain. [Color figure can be viewed in the online issue, which is available at wileyonlinelibrary.com.]

Effect of moisture content

DEM simulations yield discrete, particle level data at each time step. The discrete data can be translated into macroscopic properties of interest during flow with the use of spatial and temporal averaging methods. However, the main limitation of most averaging methods is the dependence of the values obtained on the size of control volume used.[46] Quantities such as granular temperature,[34] degree of mixing,[47] and stresses[48] have been shown to be dependent on control volume size. As discussed by Bridgwater,[47] large samples cannot detect as much variability in the measured quantities as smaller samples. Our previous computational work[22,45] showed that for dry bladed mixer flows, a plateau exists were the values of the macroscopic quantities listed above are not dependent on control volume size. It is unclear whether this is also the case for cohesive systems where particle size "alteration" occurs due to the formation of agglomerates.

Figure 5 shows the effect of control volume size on time averaged granular temperature for the dry and $\phi_{liq} = 0.045$ cases. The granular temperature is calculated from

$$T = \frac{1}{3V_{tip}^2}\langle u'u'\rangle \tag{9}$$

were u' is the localized fluctuation velocity. The mean velocity for a group of particles within a control area at a specific time is subtracted from the velocity of each particle yielding the fluctuation velocity.$\langle\rangle$ denotes the temporal averaging of the square of the fluctuation velocity of each particle. In this work, granular temperature values are normalized by V_{tip}^2. The size of the control volume (V_C) has been normalized by the volume of the 2 mm particles (V_p). The granular temperature shown in Figure 5 was obtained by averaging the fluctuation velocity in the tangential, radial and vertical directions for all the particles present in the computational domain.

Figure 5 shows a normalized granular temperature for the $\phi_{liq} = 0.045$ system which is higher than for the dry case. Figure 5 also shows that for the dry system, the granular temperature value becomes independent of control volume size for $V_C/V_p < 400$. While the granular temperature values change with control volume size for the dry system, this effect is not particularly strong since the calculated granular temperature decreased by less than 35% over the range of V_C/V_p studied. For the $\phi_{liq} = 0.045$ system, the granular temperature value continues to decrease as control volume size is decreased. This analysis shows that the formation of particle agglomerates affects the determination of macroscopic quantities via averaging. However, the granular temperature value only increases by a factor of two for the $\phi_{liq} = 0.045$ case for the whole range of $150 < V_C/V_p < 1200$ suggesting that the granular temperature is not extremely sensitive to control volume size for wet systems (similar to what was observed for dry systems). None the less, it is important to recognize that macroscopic quantities can vary with control volume size and we therefore report the control volume size in this article. The macroscopic quantities reported in the remainder of this article were obtained for fairly small control volume sizes ($V_C/V_p < 250$) where a plateau value had been reached for the dry cases.

The PIV analysis showed that particle surface velocities are significantly affected by the moisture content in the particle bed. The DEM simulations show that both the particle motion at the free surface and throughout the entire bed are affected by the amount of moisture in the system. Average radial and vertical velocity fields in front of the blades are displayed in Figure 6 for different moisture contents. The color of the vectors in Figure 6 represents the value of the tangential velocity component. A secondary flow structure consisting of a recirculation zone forms in front of the blades for all the different moisture contents studied. Particles rise by the wall forming a heap and flow downwards near the impeller shaft. The particles near the top of the heap flow radially towards the impeller while the particles near the bottom plate flow towards the cylinder wall. The development of this flow feature leads to enhanced vertical and radial mixing in dry systems.[45] The intensity of the recirculation zone changes with moisture content. For $\phi_{liq} = 0.01$ (Figure 6b) and $\phi_{liq} = 0.024$ (Figure 6c), the intensity of the recirculation zone increases when compared to the dry velocity field (Figure 6a) as radial and vertical velocities in these systems are higher. This is consistent with the PIV results presented in previous section. The increase in the intensity of the recirculation zone leads to enhanced vertical and radial mixing. The small agglomerates that form at lower moisture contents behave like highly frictional particles within the bed. Similar to the effect of microscopic friction in cohesionless systems,[45] addition of water at low moisture contents promotes convective particle motion. At high moisture contents ($\phi_{liq} = 0.045$), radial and vertical velocities decrease as can be seen in Figure 6d when compared to the dry and the lower moisture content systems. Here, the radial and vertical movement of the particles is limited by the formation of large agglomerates in front of the blades. This is also consistent with the velocity surface measurements. At this moisture content, convective particle movement is hindered by the presence of water.

Particle diffusive movement is also affected by moisture content. Normalized particle diffusivities and Peclet numbers are listed in Table 4 at different moisture contents. Particle diffusivities were calculated following the procedure outlined by Campbell[49]

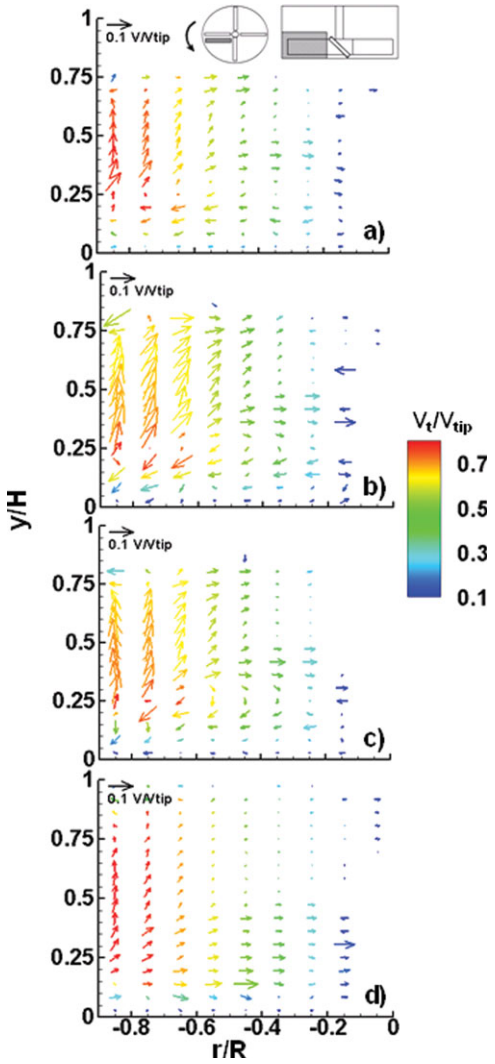

Figure 6. Effect of moisture content on velocity fields in front of the blades.

(a) dry, (b) $\phi_{liq} = 0.01$, (c) $\phi_{liq} = 0.024$, and (d) $\phi_{liq} = 0.045$. [Color figure can be viewed in the online issue, which is available at wileyonlinelibrary.com.]

$$D_{ij} = \langle (\Delta x_i - \overline{\Delta x_i})(\Delta x_j - \overline{\Delta x_j}) \rangle / 2\Delta t \tag{10}$$

where D_{ij} is the corresponding diffusion coefficient in the i direction due to a gradient in the j direction. In Eq. 10, Δx_i represents the particle displacement over a time Δt and $\overline{\Delta x_i}$ is the mean particle displacement. The mean particle displacement was calculated from the averaged distance traveled by all the particles present in the computational domain over a time Δt. Here, we normalized particle diffusivities by the tip speed of the blades and the mixer diameter, i.e., $D^*_{ij} = D_{ij}/DV_{tip}$. The diffusivity values shown in Table 4 were obtained by averaging over all the particles in the computational domain with a Δt of 1/4 revolution. The value for Δt was determined by varying this parameter until the diffusivity values that were obtained approached plateau values independent of averaging time. The presence of water at low levels ($\phi_{liq} = 0.01$ and $\phi_{liq} = 0.024$) leads to an increase in particle diffusivities when compared to the dry case diffusivities. This is consistent with the granular temperature results presented in Figure 5. The particle diffusivities in the tangential direction ($D^*_{\theta\theta}$) increase by ~30% while the diffusivities in the radial direction (D^*_{rr}) increase by ~45%. Diffusivities in the vertical direction increase the most, with the low moisture content D^*_{yy} values increasing by ~100% relative to the dry values. As moisture is added to the system, the spherical particles agglomerate to form clusters with nonspherical shapes and rough surfaces. Similar to the effect of microscopic friction observed in dry systems,[20,45] the rough surfaces of these agglomerates impart a degree of randomness in the particles' motion. The pronounced increase in D^*_{yy} values is due to an increase in the total height of the heaps that form in front of the blades. Increases in heap height for bladed mixer flows of wet particles have been observed experimentally by Lekhal et al.[33] and computationally by Radl et al.[34] The higher heap heights lead to an increase in the potential energy of the particles. This potential energy is then transferred into kinetic energy in the vertical direction as particles flow in and out of the heaps leading to the increase in particle diffusivities. A small increase in particle diffusivities is observed for the $\phi_{liq} = 0.024$ case when compared to the $\phi_{liq} = 0.01$ case.

At higher moisture contents ($\phi_{liq} = 0.045$), a different behavior is observed. The $D_{\theta\theta}$* and D_{rr}* values decrease and are lower than the dry simulation values. The D_{yy}* value decreases compared to the low moisture content cases ($\phi_{liq} = 0.01$ and $\phi_{liq} = 0.024$); but this value is higher than for the dry simulation due to the increased heap height at $\phi_{liq} = 0.045$. These results show that, while a small amount of water promotes diffusive mixing in bladed mixers, high moisture contents hinders the particles' diffusive motion.

Peclet numbers are also listed in Table 4. The Peclet number provides a way of comparing the convective and diffusive contributions to particle motion. The Peclet number is given by

$$Pe_{ij} = \frac{U_i R}{D_{ij}} \tag{11}$$

where U_i is the average particle speed, R is the mixer radius and D_{ij} is the corresponding diffusion coefficient. Here U_i was determined by averaging the speed of the particles present in the computational domain over 1/4 revolution. The averaging time was determined by varying this parameter until the Peclet numbers that were obtained approached a plateau values that were independent of averaging time. In all the cases studied, the Peclet numbers obtained are much higher than unity, indicating that convection is the dominating mechanism for particle transport. However, Peclet numbers decrease for the $\phi_{liq} = 0.01$ and $\phi_{liq} = 0.024$ cases when compared to the dry cases. This result suggests that a small amount of water in the system increases the contribution of the diffusive mechanism relative to the convective mechanism for particle motion. The smallest Peclet numbers for the low moisture content simulations are achieved in the vertical direction. At $\phi_{liq} = 0.045$, the Peclet

Table 4. Effect of Moisture Content on Normalized Particle Diffusivities and Peclet Number

ϕ_{liq}	$D_{\theta\theta}$*	D_{rr} *	D_{yy}*	$Pe_{\theta\theta}$	Pe_{rr}	Pe_{yy}
0	6.1×10^{-4}	3.2×10^{-4}	2.0×10^{-3}	860	163	35
0.01	8.1×10^{-4}	4.7×10^{-4}	5.2×10^{-3}	535	131	19
0.024	8.3×10^{-4}	4.8×10^{-4}	5.4×10^{-3}	523	129	18
0.045	3.5×10^{-4}	2.3×10^{-4}	3.6×10^{-3}	1277	189	18

Particle diffusivities were computed with a Δt of 1/4 of a revolution and were averaged over all the particles in the computational domain.

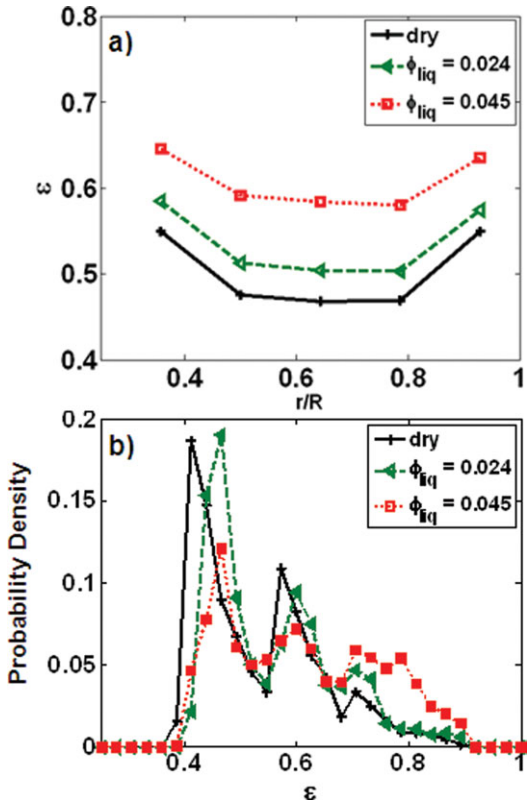

Figure 7. Effect of moisture content on void fraction within particle bed.

(a) average void fraction vs. *r*/*R* and (b) void fraction frequency distribution at steady state. [Color figure can be viewed in the online issue, which is available at wileyonlinelibrary.com.]

numbers in the tangential and radial direction increase when compared to the other cases. However, the vertical direction Peclet number is similar to the values obtained at the lower moisture contents. These results demonstrate that the diffusive behavior of particles in wet systems is complex and highly sensitive to the amount of moisture present. But, in general, high moisture contents reduce the contribution of the diffusive mechanism to particle motion.

The effect of moisture content on bed porosity is shown in Figure 7. Average void fractions at different moisture contents are plotted in Figure 7a as a function of *r*/*R*. Void fractions were calculated by creating spherical control volumes throughout the entire particle bed. The volume of the particles inside the control sphere plus the overlap volume of particles near the edges are subtracted from the volume of the control sphere to give the local void fraction. These values are then averaged in time and along the radial direction. The diameter of the spherical control volumes was 13 mm. The size of the spherical control volume was chosen by varying this parameter until the porosity values that were obtained approached plateau values that were independent of control volume size. As the moisture content in the system is increased, the void fraction within the particle bed also increases. The increase of bed porosity with moisture content was also observed in the static packing of wet spheres by Yang et al.[35] As agglomerates form in wet systems, the irregular shape and rough surfaces of the agglomerates prevent the formation of dense packed zones within the mixer increasing the overall porosity of the particle bed. The void fraction for the $\phi_{liq} = 0.045$ case increases by 13% when compared to the dry case. This is a significant change in void fraction for granular systems, where density changes of a couple of percents have been shown to cause significant differences in behavior.[50] It should be noted that the average void fraction profile obtained for the $\phi_{liq} = 0.01$ case was similar to the $\phi_{liq} = 0.024$ profile. While small differences in bed porosity may be expected between these two cases, the method for determining void fraction used here was not able to detect these differences.

The addition of water increases not only the mean void fraction within the particle bed but also the probability of larger gaps occurring in between particles. Figure 7b shows the void fraction probability frequency distributions within the bladed mixer at different moisture levels. Frequency distributions were calculated by creating spherical control volumes throughout the particle bed and calculating the void fraction in each control volume over a period of 1 revolution. The diameter of the spherical control volumes was 13 mm. For the dry system, two peaks are observed in the probability frequency distribution, one at $\varepsilon = 0.45$ and the other at $\varepsilon = 0.6$. The peak at $\varepsilon = 0.45$ represents the particles located in front of the blade, which get compressed into a denser state as the blades rotate. The peak at $\varepsilon = 0.60$ represents the particles located in the wake of the blades which are in a dilated state. Figure 7b shows a shift to the right of the graph for the wet frequency distributions when compared to the dry frequency distribution. This indicates that a larger portion of the particle bed is characterized by higher void fractions. The frequency distribution for the $\phi_{liq} = 0.045$ case shows a third peak at $\varepsilon \sim 0.75$. This peak represents the agglomerated particles located above the blades. These agglomerates posses a higher void fraction as they experience lower shearing and compressive forces above the blades.

The differences in convective and diffusive particle motion as moisture content is increased lead to differences in mixing kinetics. Degree of mixing at the different moisture contents was evaluated by coloring particles on the left side of the blade impeller differently from the particles on the right side before blade movement.[22] A statistical analysis of particle concentration for a specific color particle is then performed. At a particular time step, the relative standard deviation (RSD) of the particle concentration within the mixer is computed. The RSD is obtained from the following formula

$$\mathrm{RSD} = \frac{\sigma_{\mathrm{conc}}}{M_{\mathrm{conc}}} \tag{12}$$

where σ_{conc} is the standard deviation of the particle concentration for a specific color over all the samples taken, and M_{conc} is the overall mean concentration of the specific color particles. The size of the control volume used for the RSD calculation was $V_c/V_p = 240$. RSD values as a function of number of revolutions are shown in Figure 8a for the different cases studied. Better mixing is observed for the lower moisture content cases ($\phi_{liq} = 0.01$ and $\phi_{liq} = 0.024$) when compared to the dry, base case simulation. At these moisture contents, the formation of small agglomerate increases convective and diffusive particle motion leading to enhanced mixing. This effect is analogous to the enhancement observed in mixing kinetics for cohesive flows in rotating drums at low Bond

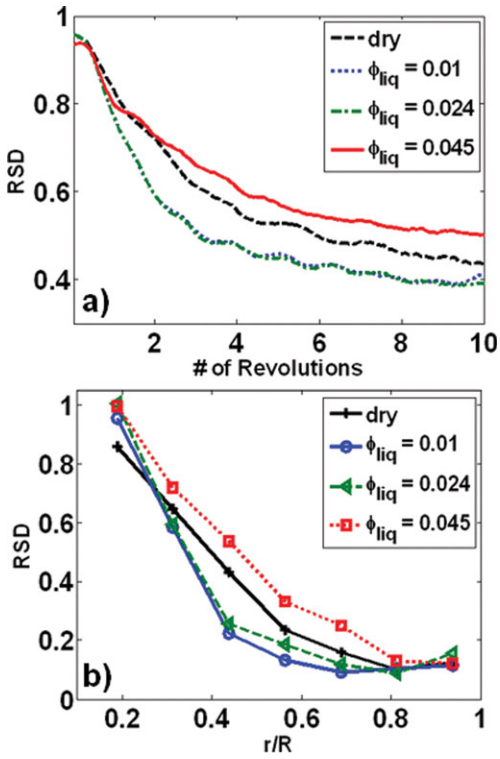

Figure 8. Effect of moisture content on mixing.

(a) RSD vs. number of revolution and (b) RSD vs. *r/R* after 10 revolutions. [Color figure can be viewed in the online issue, which is available at wileyonlinelibrary.com.]

numbers (i.e., lower amount of cohesion).[43,51] The RSD curves for the $\phi_{liq} = 0.01$ and $\phi_{liq} = 0.024$ cases lie on top of each other indicating that similar mixing kinetics are obtained for these systems. Mixing in these systems is fast with RSD values starting to level off after approximately five revolutions. A decrease in mixing performance is observed for the $\phi_{liq} = 0.045$ case. For this case, larger agglomerates form which are less mobile than the smaller agglomerates and hinder convective and diffusive particle motion. The formation of these larger agglomerates leads to a decrease in the degree of mixing. This effect is analogous to the decrease in mixing kinetics observed in rotating drums at high Bond numbers (i.e., higher amount of cohesion).[43,51]

Figure 8b shows the localized RSD values for the different cases as a function of r/R after 10 revolutions. Close to the wall ($r/R > 0.8$), the RSD values are the lowest with similar values obtained for all the different cases. This is due to the shearing action of the blades and the cylinder wall which leads to faster mixing in this region. Away from the wall however, RSD values increase and differences in the local RSD values are observed between the different cases. The low moisture content cases are characterized by a higher degree of mixing than the dry and high moisture content cases. RSD values are the highest for the $\phi_{liq} = 0.045$ case. This analysis shows the main effect of moisture content on mixing is to alter localized mixing rates for the particles located far away from the walls. It is interesting to note that Radl et al.[34] did not observe significant differences in the overall mixing rates of dry systems vs. wet systems with a relatively small amount of moisture, $\phi_{liq} = 0.007$ and Bond numbers of 2. The authors did observe differences in the localized mixing rates. Here we show that systems with a higher degree of cohesion (higher Bond numbers and higher moisture contents) mix at different rates, both locally and globally, when compared to dry systems.

We have also studied the effect of microscopic friction on the dynamics of wet flows in bladed mixers. We observe that similar to our previous work on dry systems,[45] increasing microscopic friction leads to an increase in convective and diffusive particle motion which results in enhanced mixing.[52]

Pressure and shear stress profiles

We now discuss the normal and shear stress profiles that develop inside bladed mixers for systems at different moisture contents. Stresses were calculated following the procedure outlined by Campbell.[53] Collisional stresses are obtained from

$$\tau_{ij} = \frac{1}{V_c}\langle F_i k_j \rangle \tag{13}$$

where F_i is the total contact force and k_j is the vector connecting the centers of the colliding particles. $\langle\rangle$ represents the temporal averaging within the control volume. The size of the control volume used here for the stress tensor calculations was $V_C/V_p = 120$. In this work, only the contribution of collisional stresses is considered since kinetic stresses were found to be three orders of magnitude smaller.

The collisional stresses were calculated in a 3-D cylindrical coordinate system which yielded a symmetric stress tensor (i.e., $\tau_{\theta r} = \tau_{r\theta}$). In this analysis, we focused on the average normal stress and the shear stress component in the plane of the blade rotation ($\tau_{\theta r}$). From the normal stresses, the pressure inside the particle bed is given by

$$P = \frac{1}{3}(\tau_{\theta\theta} + \tau_{rr} + \tau_{yy}) \tag{14}$$

where $\tau_{\theta\theta}$, τ_{rr}, and τ_{yy} are the normal stresses in the tangential, radial and vertical direction, respectively. Pressure and shear stress values shown here have been normalized by the quantity $\rho_p g H$, where ρ_p is the particle density and H is the maximum height of the particle bed. Figure 9a shows the normalized pressure ($P^* = P/\rho_p g H$) as a function of y/H at different moisture contents. For all the cases studied, normalized pressure increases linearly towards the bottom of the mixer since the particles at the bottom sustain the weight of the particles at the top. Similar to what is observed in dry systems, at low fill levels, the pressure profile in wet systems can be approximated by hydrostatics. Figure 9a also shows that for the $\phi_{liq} = 0.045$, the normalized pressure is lower towards the bottom of the mixer and higher towards the top. This is due to the increase in bed porosity at this moisture content. The pressure profile for the $\phi_{liq} = 0.024$ is very similar to the dry pressure profile. Although differences in bed porosity were observed at $\phi_{liq} = 0.024$, the method used to calculate stresses is not able to detect small differences in the pressure profile at this moisture content vs. the dry case.

Figure 9b shows normalized shear stress ($\tau^*_{\theta r} = \tau_{\theta r}/\rho_p g H$) profiles as a function of r/R at the different moisture contents. In all cases the values of $\tau_{\theta r}$ are highest near the cylinder wall and close to zero near the impeller shaft. This is due to the increased tangential movement observed near the wall and the increased strength of the force chains due to

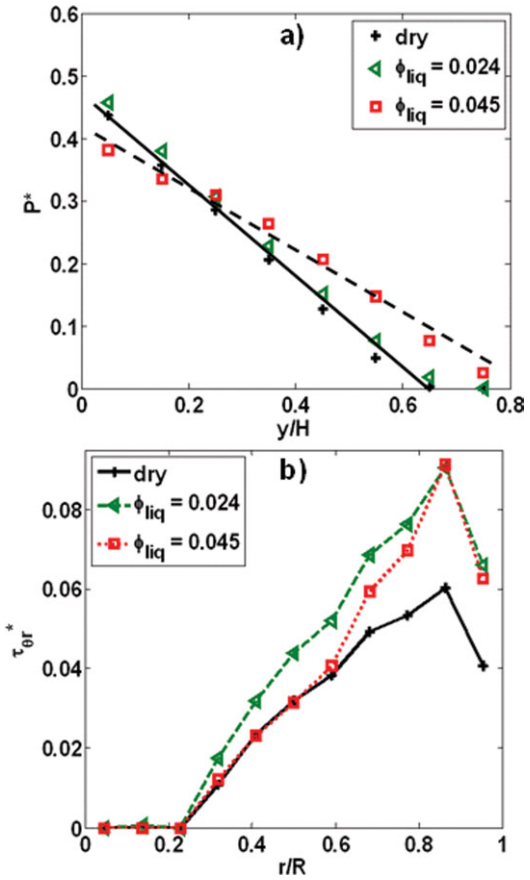

Figure 9. Effect of moisture content on normalized pressure and shear stress.

(a) time average *P vs. normalized height and (b) time average $\tau_{\theta r}$* vs. normalized radial position. [Color figure can be viewed in the online issue, which is available at wileyonlinelibrary.com.]**

wall friction. At a low moisture content ($\phi_{liq} = 0.024$), $\tau_{\theta r}^{*}$ values increased when compared to the dry values. This effect is more pronounced by the cylinder wall, where $\tau_{\theta r}$* values are ~50% higher than the dry case values. The formation of small agglomerates increases the roughness of the particle bed leading to an increase in shear stress. Increases in shear stress in wet systems have been previously observed experimentally by Pierrat et al.[1,54] via shear cell analysis and Karmakar et al.[55] via use of a soil rheometer. The shear stress analysis indicates that the addition of water at low levels enables the transfer of energy from the blades into the particle bed. This explains the increase in particle velocities observed at low moisture contents. A different behavior is observed at $\phi_{liq} = 0.045$. In this case, $\tau_{\theta r}$* values by the walls are similar to the $\phi_{liq} = 0.024$ values. However, the $\tau_{\theta r}$* values decrease towards the center of the particle bed and are similar to the dry case values. The decrease in mixing rates towards the center of the particle bed at high moisture contents can also be explained in the context of the shear stress profiles. As larger agglomerates are formed at higher moisture contents, a larger amount of energy is needed to break the agglomerates and to promote mixing. Since a lower amount of energy is transferred from the blades to the particle bed in this central region, the large agglomerates remain and mixing is decreased.

In addition to affecting average stress values, moisture content affects the distribution of forces throughout the particle bed. Figure 10 shows instantaneous normal contact force networks in the horizontal plane for the dry case (Figure 10a) and the $\phi_{liq} = 0.045$ case (Figure 10b). In Figure 10, each line represents the contact vector connecting the center of the particles and the thickness of the line represents the magnitude of the normal force associated with that contact. Higher forces are represented by thicker lines and vice versa. Here, only the particle contacts located near the top half of the particle bed are displayed, as shown by the side view drawing in Figure 10. The contact force network for the dry simulation is fairly homogeneous while the network for the $\phi_{liq} = 0.045$ simulation is very heterogeneous. Stronger contact chains which extend further into the particle bed are observed for the wet case. A similar behavior was observed by Yang et al.[35] in the static packing of wet spheres. At high moisture contents, the magnitude of the capillary forces increases which causes the increase in normal forces and, consequently, the formation of large agglomerates. The white areas shown in Figure 10b represent areas of high bed porosity just behind the blade where no particles are present. Thus, the contact force network for the $\phi_{liq} = 0.045$ simulation displays the roughness of the particle bed surface while the dry case network shows the smooth surface of the bed.

Effect of moisture content on particle agglomeration

The effect of moisture content on the formation of agglomerates in bladed mixers is discussed in this section. A method was developed to evaluate the extent of agglomeration that occurs in the bladed mixer at different moisture contents. In this method, the contact time (t_c) for each particle–particle contact is tracked during shearing. In the wet simulations, particles are considered to be in contact if the surfaces of the particles had been in contact at some previous time and if the distance between the surfaces of the particles is less than the rupture distance of the liquid bridge ($\widehat{h}_c R$) since the time of initial contact. Tracking of contact time is started after the system has reached steady-state (~2 to 3 sec after the blades are set to rotate). From the dry simulation, a characteristic time-of-contact breakage is determined (t_{break}^{dry}). t_{break}^{dry} represents the amount of time that it takes the shearing action of the blades to break all the particle–particle contacts that were present at a particular time step in the dry system. If a particle–particle contact in the

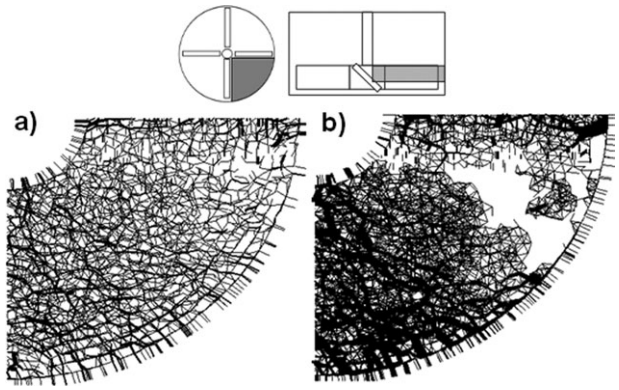

Figure 10. Effect of moisture content on normal contact force network near top of the blades.

(a) dry and (b) $\phi_{liq} = 0.045$.

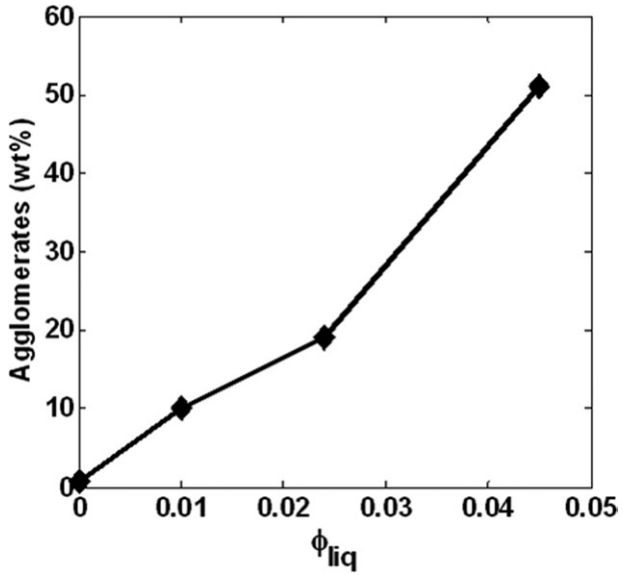

Figure 11. Weight percent of particle agglomeration vs. moisture content at steady state.

wet simulation is characterized by $t_c > t_{break}^{dry}$, then this contact is classified as an enduring wet contact and these particles are considered to be agglomerated. Groups of agglomerated particles are then determined from the list of enduring wet contacts. From the list of enduring contacts, a "neighbor" list for each particle is compiled. These neighbor lists are then compared across the entire system to determine the number of particles present in each agglomerate. For the simulation conditions used here, t_{break}^{dry} was chosen to be one revolution. This is equal to 4 blade passes for the blade configuration shown in Figure 1. The of value t_{break}^{dry} was determined by varying this parameter until the average agglomerate size obtained from the particle tracking was independent of t_{break}^{dry}.

Figure 11 shows the weight percent of the particle bed which is agglomerated at different moisture contents based on the method described earlier. With this method, no agglomeration is obtained for the dry system (i.e., $\phi_{liq} = 0$) as can be seen from Figure 11. As moisture content is increased, the weight percent of the particle bed which is agglomerated increases. For $\phi_{liq} = 0.045$, roughly 50% of the particle bed is agglomerated. This shows that a significant amount of agglomeration can occur in bladed mixers at high Bond numbers and modest moisture contents despite the significant amount of shearing provided by the blades. It should be noted that the values listed in Figure 11 do not change at steady state since, for the wet simulations, we assume a perfect liquid distribution within the mixer.

The effect of moisture content on the size of the agglomerates at steady state is shown in Figure 12. As expected, increasing moisture content increases the size of agglomerates as a higher amount of energy is needed to break the liquid bridges that exist between particles. Average agglomerate size vs. r/R is shown in Figure 12a at the different moisture contents. Larger agglomerates are obtained close to the impeller shaft and agglomerate size decreases towards the cylinder wall. Figure 9b shows that stresses are higher near the cylinder wall leading to the formation of smaller agglomerates in this region. This is consistent with the agglomeration behavior observed in wet shear flows, where the extent of agglomeration is reduced when the amount of shearing is increased.[25,26] Similar agglomerate sizes are observed near the cylinder wall at the different moisture contents since similar $\tau_{\theta r}$* values are obtained in this region. The differences in agglomerate size along the radial direction explain the reduction in mixing rates for the $\phi_{liq} = 0.045$ case. Close to the wall, the majority of the agglomerates formed are small (between 2-4 particles in size). These small agglomerates increase the roughness of the particle bed leading to enhanced mixing in this region. Towards the center of the particle bed, agglomerates with an average size of ~35 particles are formed. These large agglomerates hinder particle motion in the radial and vertical direction (as shown in Figure 6) leading to a decrease in mixing.

Average agglomerate size vs. y/H is shown in Figure 12b at the different moisture contents. Here again we see that increasing moisture content increases the average size of the agglomerates. Smaller agglomerates are observed near the cylinder's bottom plate and agglomerate size increases towards the top of the particle bed. The formation of small agglomerates towards the bottom is due to the increased pressure in this region. As the particles near the bottom

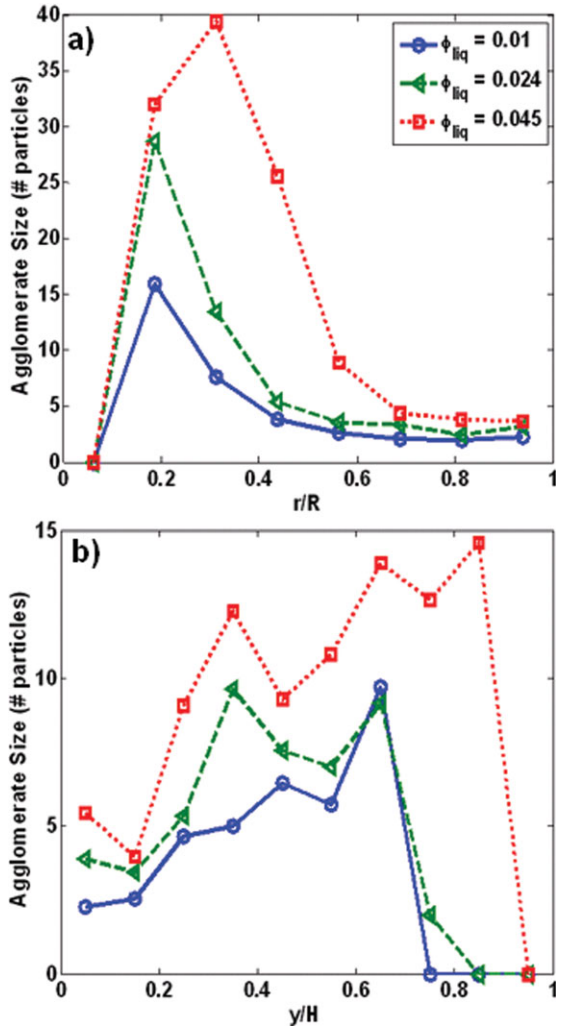

Figure 12. Effect of moisture content on average agglomerate size.

(a) agglomerate size vs. r/R and (b) agglomerate size vs. y/H. [Color figure can be viewed in the online issue, which is available at wileyonlinelibrary.com.]

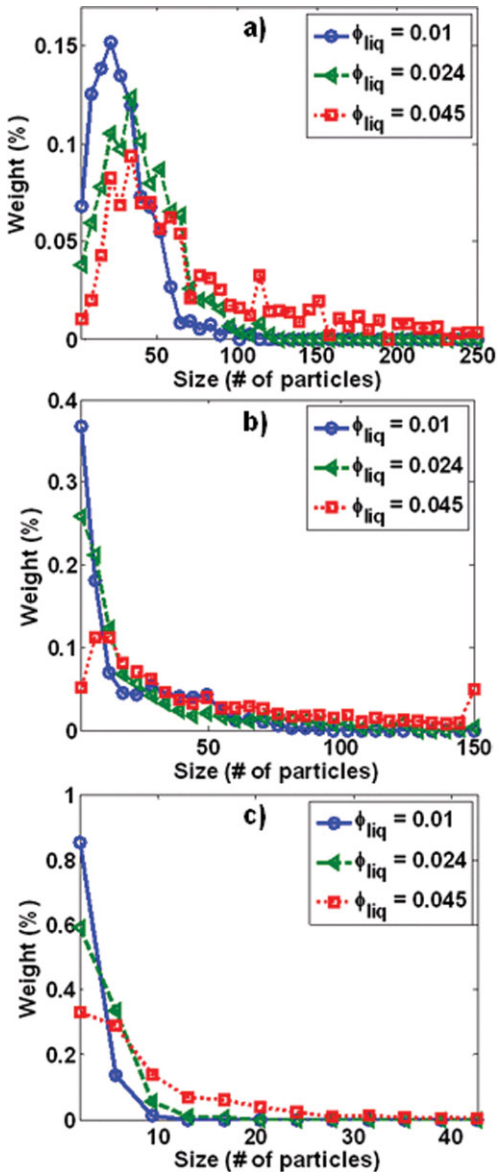

Figure 13. Effect of moisture content on agglomerate particle-size distribution.

(a) size distribution near impeller shaft, (b) size distribution in the center, and (c) size distribution near cylinder wall. Note: The lower limit of the abscissa for these graphs is 2 since only the agglomerated particles are considered in this analysis. [Color figure can be viewed in the online issue, which is available at wileyonlinelibrary.com.]

sustain the weight of the particles near the top, the agglomerates that form towards the bottom experience higher normal and shear stresses and therefore large agglomerates cannot form.

Differences in the size distribution of the agglomerates at steady state were also obtained. Figure 13 displays the agglomerate size distributions obtained at different locations within the particle bed with the different moisture contents. The lower limit of the abscissa for the graphs shown in Figure 13 is 2 since only the agglomerated particles are considered in this analysis. Figure 13 shows that the shape of the agglomerate size distribution is not constant throughout the particle bed. Near the impeller shaft (Figure 13a), right-skewed size distributions are obtained while towards the center of the bed (Figure 13b) and near the cylinder walls (Figure 13c), lognormal distributions are obtained. The agglomerate size distribution near the impeller shaft shifts to the right and becomes broader as moisture content is increased. As can be seen from Figure 13a, agglomerates containing more than 150 particles are obtained for the $\phi_{liq} = 0.045$ case even though the average agglomerate size is ~35. The presence of these large agglomerates coupled with the lower shear stresses lead to reduced mixing in this region. For the remainder of the particle bed, lognormal agglomerate size distributions are obtained. The amount of agglomerates composed of two particles is reduced as moisture content is increased leading to broader distributions in the center of the particle bed and near the cylinder walls. For the $\phi_{liq} = 0.045$ case, ~5 wt % of agglomerates contain 150 particles or more in the center of the particle bed. The agglomerate particle-size distributions are smallest near the cylinder wall. Here, the majority of the agglomerates are composed of two particles although agglomerates composed of >20 particles are observed for the $\phi_{liq} = 0.045$ case.

Finally, we look at the effect of moisture content on agglomerate shape. Figure 14a displays the average agglomerate aspect ratio as a function of r/R. Aspect ratio is defined as the ratio of the length of the major axis to the length of the minor axis. For agglomerates composed of multiple particles, the aspect ratio is calculated by determining the distance between each particle and the center of mass of the agglomerate. From these distances the length of the major and minor axis is determined. A lower aspect ratio represents a more symmetrical shape (as spheres have an aspect ratio of 1) while a larger aspect ratio represents a more elongated particle shape. As can be seen in Figure 14, the average aspect ratio of the agglomerates increases as moisture content is increased. This means that agglomerates with more elongated, needle-like shapes are formed at higher moisture contents. Figure 14a also shows that the shape of the agglomerates is not constant throughout the particle bed. Aspect ratio is highest by the impeller shaft and decreases towards the cylinder walls since higher stresses in this region prevent the formation of longer agglomerates.

In Figure 14b, the morphology of some agglomerates that form in the different regions of the particle bed is displayed. These agglomerates have a size and aspect ratio which is similar to the average values obtained at the different moisture contents. The size of the agglomerates increases as moisture content is increased which is consistent with the results presented in this section. Near the impeller shaft, elongated agglomerates are observed while shorter agglomerates are formed closer to the cylinder walls. The smaller agglomerates form as elongated agglomerates are broken along the major axis by the shearing action of the blades into shorter agglomerates. This is similar to the fracture of needle-like particles due to shearing.

The results presented here show that while a more complex behavior is obtained in wet flows, many of the trends observed are consistent with the behavior observed in dry systems. At low moisture contents, the formation of small agglomerates increases the roughness of the particle bed. These "rough," wet particle beds show a behavior similar to that of frictional, dry particle beds. At higher moisture contents however, the behavior differs. Larger agglomerates are formed reducing the mobility of the particles within the mixer and significantly affecting the distribution of stress within the particle bed.

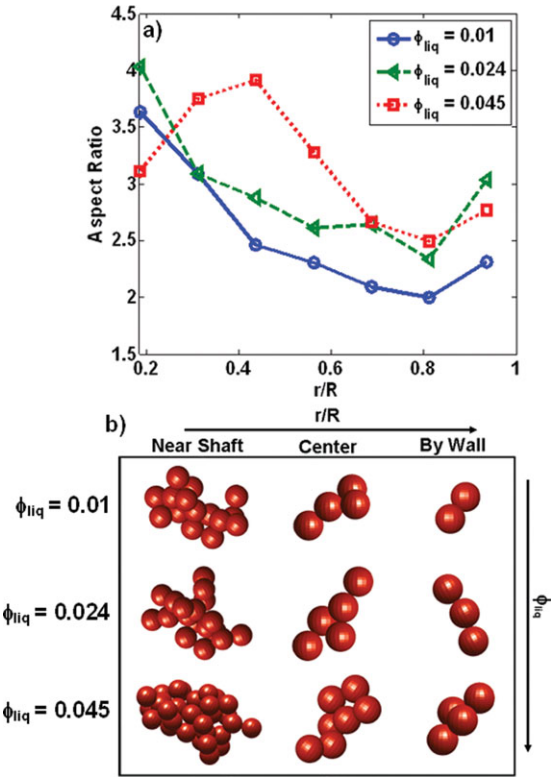

Figure 14. Effect of moisture content on agglomerate shape.

(a) average agglomerate aspect ratio vs. *r*/*R* and (b) agglomerate morphology at different moisture content. [Color figure can be viewed in the online issue, which is available at wileyonlinelibrary.com.]

Conclusions

Experimental and computational methods were used to study the behavior of wet particle flows in bladed mixers. The ability of DEM simulations to qualitatively capture experimental behavior was demonstrated. Particle velocities profiles obtained from the simulations are in good qualitative agreement with those obtained experimentally using the PIV technique. The discrepancies observed between the simulation results and the experimental results could be due to differences in particle properties, wall friction and the slight polydispersity present in the glass beads used (but not accounted for in the simulations). Additionally in the simulations the water is assumed to uniformly coat the particles and be perfectly mixed within the particle bed. Some of the discrepancies observed at higher moisture contents could be the result of water accumulation near the bottom of the cylinder in the experiments due to the low viscosity of water. While this effect is not accounted for in the simulation, the general trends observed in the simulations are similar to the experimental trends. Further work is needed to study the effect of liquid viscosity on liquid dispersion in bladed mixers.

DEM simulation results showed that addition of water at low moisture contents leads to an increase in the radial and vertical velocities of the particles located in front of the blades leading to a stronger recirculation pattern than what is observed in the dry system. Particle diffusivities also increase at low moisture contents. The increase in convective and diffusive particle motion at low moisture contents leads to enhanced mixing kinetics when compared to the dry case. However, at higher moisture contents the behavior changes. In this case, the presence of water leads to lower radial and vertical particle velocities in front of the blades. Particle diffusivities also decrease. This decrease in particle motion leads to lower mixing rates at high moisture contents. Bed porosity was shown to increase as moisture content is increased. Void fraction increases by 12% for the high moisture content simulation when compared to the dry simulation.

Pressure and shear stress profiles are significantly affected by moisture content. The average pressure inside the particle bed at different moisture contents was shown to be linear and approximated by hydrostatics. Shear stress was highest near the cylinder wall and lowest by the impeller shaft for all the cases studied. At low moisture contents, higher shear stresses were obtained compared to the dry systems. For high moisture contents, the stresses near the cylinder wall are high. However, shear stress decreases towards the center of the particle bed with values similar to those obtained for the dry case.

The cohesive forces that develop in wet systems lead to the formation of particle clusters or agglomerates. A method for examining the extent of agglomeration in the wet particle simulations was developed. Our analysis showed that the portion of the particle bed which is agglomerated increases as moisture content is increased. At the highest moisture content examined, close to 50% of the particles in the system were agglomerated. Agglomerate size is highest near the impeller shaft and towards the top of the particle bed, regions characterized by lower stresses. A strong dependence between the aspect ratio of the agglomerates and moisture content was found. Aspect ratio increases with moisture content indicating the formation of elongated, needle-like agglomerates.

This work described the behavior of an idealized, wet granular system (nonporous monodisperse spheres with a perfect liquid distribution) in a bladed mixer. While simple in nature, it represents an initial step towards understanding flow, mixing and agglomeration of wet granular systems. Further work is needed to examine the effect of mixer size and other operating parameters on the trends reported here.

Acknowledgments

B.R. thank Bristol-Myers Squibb for the financial support during an educational leave of absence. The authors thank T. M. Canty, M. Gsöll, and O. Isijola for their assistance. This work was partially supported by the National Science Foundation and DEM Solutions.

Notation

m_i = mass of particle i
R_i = radius of particle i
I_i = moment of inertial of particle i
v_i = velocity of particle i
g = acceleration due to gravity
F_{ij}^N = normal force resulting from the contact of particle i with particle j
F_{ij}^T = tangential force resulting from the contact of particle i with particle j
F_{ij}^C = cohesive force experienced by particle i due to a liquid bridge with particle j
d = particle diameter
E = Young's modulus
e = coefficient of restitution

$\widehat{V}$ = dimensionless liquid bridge volume
$\widehat{h}$ = dimensionless separation distance between surface of particles
$\widehat{h}_c$ = critical rupture distance for liquid bridge
Ca = capillary number
U = characteristic system velocity
V_{tip} = tip speed of blades
u' = localized fluctuation velocity
T = normalized granular temperature
V_c = control volume size
V_p = particle volume
D_{ij} = diffusion coefficient in the i direction due to a gradient in the j direction
$\underline{\Delta x_i}$ = particle displacement in the i direction
$\overline{\Delta x_i}$ = mean particle displacement in the i direction
Pe = Peclet number
U_i = average particle speed
M_{conc} = mean particle concentration
P^* = normalized pressure
t_c = particle–particle contact time
t_{break}^{dry} = characteristic time-of-contact breakage for dry system

Greek Letters

ω_i = angular velocity of particle i
ρ_p = particle density
σ = Poisson ratio
μ_r = rolling friction coefficient
μ_s = silding friction coefficient
τ_{rij} = torque resulting from the contact of particle i with particle j
β = half filling angle of a capillary liquid bridge
θ = contact angle of a capillary liquid bridge
γ = surface tension of liquid
ρ_{liq} = density of liquid in a capillary liquid bridge
ϕ_{liq} = volume fraction of liquid in wet systems
η = dynamic viscosity of liquid
ε = void fraction
σ_{conc} = standard deviation of particle concentration
τ_{ij} = stress on i plane in the j direction
τ_{ij}^* = normalized shear stress

Literature Cited

1. Pierrat P, Caram HS. Tensile strength of wet granular materials. *Powder Technol*. 1997;91:83–93.
2. Schulz M, Schulz BM, Herminghaus S. Shear-induced solid-fluid transition in a wet granular medium. *Phys Rev E: Stat Nonlinear Soft Matter Phys.* 2003;67:52301–52301.
3. Herminghaus S. Dynamics of wet granular matter. *Adv Phys*. 2005;54:221–226.
4. Alexander AW, Chaudhuri B, Faqih A, Muzzio FJ, Davies C, Tomassone MS. Avalanching flow of cohesive powders. *Powder Technol*. 2006;164:13–21.
5. Faqih A, Chaudhuri B, Muzzio FJ, Tomassone MS, Alexander A, Hammond S. Flow—induced dilation of cohesive granular materials. *AIChE J*. 2006;52:4124–4132.
6. Rognon PG, Roux JN, Naaim M, Chevoir F. Dense flows of cohesive granular materials. *J Fluid Mech*. 2008;596:21–47.
7. Tomas J. Fundamentals of cohesive powder consolidation and flow. *Granular Matter*. 2004;6:75–86.
8. Wibowo C, Ng KM. Operational issues in solids processing plants: systems view. *AIChE J*. 2001;47:107–125.
9. Begat P, Morton DAV, Staniforth JN, Price R. The cohesive-adhesive balances in dry powder inhaler formulations i: direct quantification by atomic force microscopy. *Pharm Res.* 2004;21:1591–1597.
10. Willett CD, Adams MJ, Johnson SA, Seville JPK. Capillary bridges between two spherical bodies. *Langmuir*. 2000;16:9396–9405.
11. Papadakis SE, Bahu RE. Sticky issues of drying. *Drying Technol*. 1992;10:817–837.
12. Muguruma Y, Tanaka T, Tsuji Y. Numerical simulation of particulate flow with liquid bridge between particles (simulation of centrifugal tumbling granulator). *Powder Technol*. 2000;109:49–57.
13. Muzzio FJ, Alexander A, Goodridge C, Shen E, Shinbrot T. *Solids mixing part a: fundamentals of solids mixing*. In: Paul EL, Atiemo-Obeng V, Kresta SM, editors. *Handbook of Industrial Mixing: Science and Practice*. Hoboken, NJ: Wiley, 2004: 887–983.
14. Faure A, York P, Rowe RC. Process control and scale-up of pharmaceutical wet granulation processes: a review. *Eur J Pharm Biopharm*. 2001;52:269–277.
15. Gantt JA, Cameron IT, Litster JD, Gatzke EP. Determination of coalescence kernels for high-shear granulation using DEM simulations. *Powder Technol*. 2006;170:53–63.
16. Litster JD. Scaleup of wet granulation processes: science not art. *Powder Technol*. 2003;130:35–40.
17. Lee T, Lee J. Particle attrition by particle-surface friction in dryers. *Pharm Technol*. 2003;27:64–72.
18. Lekhal A, Girard KP, Brown MA, Kiang S, Glasser BJ, Khinast JG. Impact of agitated drying on crystal morphology: KCl-water system. *Powder Technol*. 2003;132:119–130.
19. Lekhal A, Girard KP, Brown MA, Kiang S, Khinast JG, Glasser BJ. The effect of agitated drying on the morphology of -threonine (needle-like) crystals. *Int J Pharm*. 2004;270:263–277.
20. Remy B, Canty TM, Khinast JG, Glasser BJ. Experiments and simulations of cohesionless particles with varying roughness in a bladed mixer. *Chem Eng Sci*. 2010;65:4557–4571.
21. Conway SL, Lekhal A, Khinast JG, Glasser BJ. Granular flow and segregation in a four-bladed mixer. *Chem Eng Sci*. 2005;60:7091–7107.
22. Remy B, Khinast JG, Glasser BJ. The effect of mixer properties and fill level on granular flow in a bladed mixer. *AIChE J*. 2010;56:336–353.
23. Stewart RL, Bridgwater J, Parker DJ. Granular flow over a flat-bladed stirrer. *Chem Eng Sci*. 2001;56:4257–4271.
24. Chandratilleke GR, Yu AB, Stewart RL, Bridgwater J. Effects of blade rake angle and gap on particle mixing in a cylindrical mixer. *Powder Technol*. 2009;193:303–311.
25. Kantak AA, Hrenya CM, Davis RH. Initial rates of aggregation for dilute, granular flows of wet particles. *Phys Fluids*. 2009;21:023301–023313.
26. Khan MI, Tardos GI. Stability of wet agglomerates in granular shear flows. *J Fluid Mech*. 1997;347:347–368.
27. Anand A, Curtis JS, Wassgren CR, Hancock BC, Ketterhagen WR. Predicting discharge dynamics of wet cohesive particles from a rectangular hopper using the discrete element method (DEM). *Chem Eng Sci*. 2009;64:5268–5275.
28. Deliang S, McCarthy JJ. Numerical simulation of liquid transfer between particles. *Powder Technol*. 2008;184:64–75.
29. Li H, McCarthy JJ. Controlling cohesive particle mixing and segregation. *Phys Rev Lett*. 2003;90:184301–184301.
30. Rahmanian N, Ghadiri M, Ding Y. Effect of scale of operation on granule strength in high shear granulators. *Chem Eng Sci*. 2008;63:915–923.
31. Sato Y, Okamoto T, Watano S. Scale-up of high shear granulation based on agitation power. *Chem Pharm Bull*. 2005;53:1547–1550.
32. Sirois P, Craig G. Scaleup of a high-shear granulation process using a normalized impeller work parameter. *Pharm Dev Technol*. 2000;5:365.
33. Lekhal A, Conway SL, Glasser BJ, Khinast JG. Characterization of granular flow of wet solids in a bladed mixer. *AIChE J*. 2006; 52:2757–2766.
34. Radl S, Kalvoda E, Glasser BJ, Khinast JG. Mixing characteristics of wet granular matter in a bladed mixer. *Powder Technol*. 2010; 200:171–189.
35. Yang RY, Zou RP, Yu AB. Numerical study of the packing of wet coarse uniform spheres. *AIChE J*. 2003;49:1656–1666.
36. Anand A, Curtis JS, Wassgren CR, Hancock BC, Ketterhagen WR. Segregation of cohesive granular materials during discharge from a rectangular hopper. *Granular Matter*. 2010;12:193–200.
37. Tsuji Y, Tanaka T, Ishida T. Lagrangian numerical simulation of plug flow of cohesionless particles in a horizontal pipe. *Powder Technol*. 1992;71:239–250.
38. Mikami T, Kamiya H, Horio M. Numerical simulation of cohesive powder behavior in a fluidized bed. *Chem Eng Sci*. 1998;53:1927–1940.
39. Richefeu V, Youssoufi MSE, Radjai F. Shear strength properties of wet granular materials. *Phys Rev E: Stat Nonlinear Soft Matter Phys*. 2006;73:51304–51301.
40. Lian G, Thornton C, Adams MJ. A theoretical study of the liquid bridge forces between two rigid spherical bodies. *J Colloid Interface Sci*. 1993;161:138–147.
41. Scheel M, Seemann R, Brinkmann M, Di Michiel M, Sheppard A, Breidenbach B, Herminghaus S. Morphological clues to wet granular pilestability. *Nat Mater*. 2008;7:189–193.
42. Shi D, McCarthy JJ. Numerical simulation of liquid transfer between particles. *Powder Technol*. 2008;184:64–75.

43. McCarthy JJ. Micro-modeling of cohesive mixing processes. *Powder Technol.* 2003;138:63–67.
44. Donahue CM, Hrenya CM, Davis RH, Nakagawa KJ, Zelinskaya AP, Joseph GG. Stokes' Cradle: normal three-body collisions between wetted particles. *J Fluid Mech.* 2010;650:479–504.
45. Remy B, Khinast JG, Glasser BJ. Discrete element simulation of free flowing grains in a four-bladed mixer. *AIChE J.* 2009;55:2035–2048.
46. Zhu HP, Zhou ZY, Yang RY, Yu AB. Discrete particle simulation of particulate systems: theoretical developments. *Chem Eng Sci.* 2007;62:3378–3396.
47. Bridgwater J. The dynamics of granular materials—towards grasping the fundamentals. *Granular Matter.* 2003;4:175–181.
48. Glasser BJ, Goldhirsh I. Scale dependence, correlations, and fluctuations of stresses in rapid granular flows. *Phys Fluids.* 2001;13:407–420.
49. Campbell CS. Self-diffusion in granular shear flows. *J. Fluid Mech.* 1997;348:85–101.
50. Langroudi MK, Tardos GI, Michaels JN, Mort P. Effect of material properties, boundary conditions and flow fields on the rheology of dense granular matter. Paper Presented at the Powders and Grains 2009: Proceedings of the 6th International Conference on Micromechanics of Granular Media, 2009; Golden (Colorado).
51. Chaudhuri B, Mehrotra A, Muzzio FJ, Tomassone MS. Cohesive effects in powder mixing in a tumbling blender. *Powder Technol.* 2006;165:105–114.
52. Remy B. *Granular Flow, Segregation and Agglomeration in Bladed Mixers*. New Brunswick: Chemical and Biochemical Engineering, Rutgers, The State University of New Jersey, 2010.
53. Campbell CS. Granular shear flows at the elastic limit. *J. Fluid Mech.* 2002;465:261–291.
54. Pierrat P, Agrawal DK, Caram HS. Effect of moisture on the yield locus of granular materials: theory of shift. *Powder Technol.* 1998;99:220–227.
55. Karmakar S, Kushwaha RL. Development and laboratory evaluation of a rheometer for soil visco-plastic parameters. *J Terramechan.* 2007;44:197–204.

Manuscript received Aug. 11, 2011, and revision received Dec. 11, 2011.